

# Inosine pranobex-derived coordination complexes for self-adjuvant, self-carrier, and self-assembled vaccines in cancer immunotherapy

Xia Li<sup>a\*</sup>, Shinya Hattori<sup>b</sup>, Tomohiko Yamazaki<sup>a</sup>, Mitsuhiro Ebara<sup>a</sup>, Naoto Shirahata<sup>c,d</sup>, Nobutaka Hanagata<sup>a</sup>

<sup>a</sup> Research Center for Macromolecules and Biomaterials, National Institute for Materials Science, 1-1 Namiki, Tsukuba, Ibaraki 305-0044, Japan,

<sup>b</sup> Bioanalysis Unit, Research Network and Facility Services Division, National Institute for Materials Science, Tsukuba, Ibaraki, Japan,

<sup>c</sup> Research Center for Materials Nanoarchitectonics (MANA), National Institute for Materials Science, 1-1 Namiki, Tsukuba, Ibaraki 305-0044, Japan,

<sup>d</sup> Graduate School of Chemical Sciences and Engineering, Hokkaido University, Sapporo, Japan

E-mail: [LI.Xia@nims.go.jp](mailto:LI.Xia@nims.go.jp)

**Abstract:** Inosine pranobex (InP), an immunomodulatory drug approved for clinical use worldwide, is a potential adjuvant for cancer vaccines with a low clinical translation barrier. However, the administration of soluble InP agents in free format is associated with drawbacks of a short half-life period and low drug bioavailability. In this study, a rapid self-assembly approach was proposed for the synthesis of cancer vaccines due to the coordination interaction of ferric ion and acedoben (Ace) in InP. The self-assembled cancer vaccines can be readily adjusted from the microscale to the nanoscale, with shapes including rods, fibers, and spheres. Herein, Fe-Ace coordination complexes not only serve as carriers for tumor antigens, but also enhance antigen-specific antitumor immunity due to their intrinsic adjuvant properties. Nanofibrous self-assembled cancer vaccines based on Fe-Ace coordination complexes more effectively induced an antitumor immune response, exerted a remarkable therapeutic effect, and inhibited the tumor growth at distant site *in vivo*, compared to free InP and other self-assembled cancer vaccines. The presented work provides a promising strategy for the rapid manufacture of InP-derived self-adjuvant, self-carrier, and self-assembled vaccines for cancer immunotherapy.

**Keyword:** Cancer immunotherapy; Therapeutic cancer vaccines; Coordination complexes; Inosine pranobex; Self-assembly.

## 1. Introduction

Cancer immunotherapy attempts to utilize the exquisite power of host's immune system to prevent, control and eradicate cancer [1, 2]. In recent years, cancer immunotherapy has made rapid strides and has attracted considerable attention as a promising cancer treatment after surgery, chemotherapy, and radiotherapy [1, 3]. Cancer immunotherapy encompasses a range of modalities, including cancer vaccines, immune checkpoint inhibitors and others [4-6]. Based on their mechanism of action, cancer immunotherapy falls into two broad categories. One category aims to release the brakes by blocking negative immune regulation, such as immune checkpoint inhibitors [5]. The other category is to activate immune cells, increase their number and strengthen antitumor immunity, including cancer vaccines [4, 6, 7].

Therapeutic cancer vaccines are designed to enhance the body's immune system to detect, attack and eliminate cancer cells that express specific tumor antigens on their surface [7, 8]. Adjuvants in cancer vaccines are defined as substances that enhance tumor immunogenicity and therapeutic efficacy [9, 10]. When cancer vaccines are administered into the body, antigen-presenting cells (APCs) will accumulate at the injection site, take up them, and present them to T lymphocytes in adjacent lymph nodes, thereby triggering an adaptive antitumor immune response to eliminate cancer cells. This antitumor effect induced by cancer vaccines tends to be characterized by long-lasting and immunological memory. Nevertheless, the therapeutic efficacy of cancer vaccines is contingent upon their design principle and manufacturing technology [9, 11]. For example, the administration of antigens alone in the absence of adjuvants can easily lead to immune tolerance and thus fail to induce a robust antitumor immune response [10-12]. Even when antigens and adjuvants are administered simultaneously in free format, they rapidly diffuse and fail to generate a strong and effective efficacy [9-12]. The codelivery of antigens and adjuvants into the same antigen-presenting cells via nanotechnology is anticipated to elicit a robust antitumor immune response and enhance the efficacy of cancer vaccines [9-13]. Despite many advances that have been made in the past, it remains a challenge to develop highly effective cancer vaccines in a simple and rapid way, obtain their regulatory approval and expand their clinical use.

Inosine pranobex (InP) is an immunomodulatory drug, composed of inosine, acedoben and dimethylaminoisopropanol in a ratio of 1:3:3. Initially approved in 1971, InP is currently in clinical use in many countries worldwide [14]. InP has been reported to treat viral infections [14] and improve immune function in cancer patients [15]. This is due to its ability to stimulate the secretion of Th1-related cytokines, such as IL-2, IFN- $\gamma$  and TNF- $\alpha$ , promote the proliferation of monocytes and lymphocytes, and potentiate the function of T lymphocytes and phagocytic cells [14, 16, 17]. InP is a well-tolerated drug with no serious side effects, and its oral daily dose is generally 1 ~ 6 g for human use [14-16, 18]. However, the administration of soluble InP agents in free format is associated with drawbacks, including a short half-life period, low drug bioavailability and limited efficacy for cancer immunotherapy. Furthermore, iron plays a role in maintaining immune function [19], and iron-containing nanomaterials have been reported to inhibit tumor growth [20, 21]. The use of iron-containing nanomaterials (e.g., iron oxide, ferrous fumarate) has been approved for nuclear magnetic resonance imaging of cancer and iron supplementation [20, 22].

Herein, a rapid self-assembly strategy is employed to alter the administration formulation of InP agents and fabricate InP-derived Fe-Ace coordination complexes for the first time. During the formation of Fe-Ace coordination complexes, tumor antigens are simultaneously and uniformly encapsulated inside, forming self-adjuvant, self-carrier, and self-assembled cancer vaccines (**Scheme 1**). The self-assembled cancer vaccines can be tailored from microscale to nanoscale with various shapes. Compared with InP in free format, InP-derived self-assembled cancer vaccines are more effective in triggering tumor antigen-specific antitumor immune



15000 rpm for 10 minutes, washed once with water and used to prepare aqueous suspensions or lyophilized. The obtained self-assembled cancer vaccines synthesized in water, F127-containing aqueous solution, and PVP-containing aqueous solution were named Fe-Ace-O1, Fe-Ace-O2, and Fe-Ace-O3, respectively. To visualize the antigens, F-OVA was employed to prepare self-assembled cancer vaccines, which were designated as Fe-Ace-FO1, Fe-Ace-FO2 and Fe-Ace-FO3, respectively. To visualize the proteolysis process of the antigens, DQ-OVA was used to prepare self-assembled cancer vaccines synthesized in water and F127-containing aqueous solution, which were named Fe-Ace-DO1 and Fe-Ace-DO2, respectively.

**2.4. Physicochemical characterization.** The coordination complexes and cancer vaccines were observed using a scanning electron microscope (SEM; S-4800, Hitachi, Japan) equipped with an energy-dispersive X-ray (EDX) spectrometer. The samples were subjected to analysis via an X-ray diffraction (XRD) system with CuK $\alpha$  X-ray (RINT-Ultima III, Rigaku, Japan). The sample suspensions were tested using a zeta-potential analyzer (ELSZ-1000Z) and a dynamic light scattering spectrophotometer (DLS; DLS-8000HAL, Otsuka Electronics, Japan). The structure and composition were characterized by Fourier transform infrared spectroscopy (FTIR; IRTracer-100, Shimadzu, Japan) and X-ray photoelectron spectroscopy (XPS) with AlK $\alpha$  monochromatic X-rays of 25 W, 15 kV, and 100  $\mu$ m in diameter (Quantes, ULVAC-PHI, Inc., Japan).

The concentrations of InP in solutions were quantified using an ultraviolet-visible (UV-vis) spectrophotometer (NanoDrop 2000, Thermo Fisher Scientific Inc., USA) and a high-performance liquid chromatography-mass spectrometry (HPLC-MS) system comprising a Prominence Series HPLC (Shimadzu Corporation, Japan) and a Finnigan LXQ linear ion-trap MS (Thermo Fisher Scientific Inc., USA). The concentrations of OVA in solutions are quantified via a Micro BCA protein assay kit (Thermo Fisher Scientific Inc., USA). The loading efficiencies are determined by the percentages of the amount of loaded biomolecules to the total amount of biomolecules added.

**2.5. Cellular uptake.** The primary dendritic cells (DCs) were obtained from bone marrow according to the previously reported methodology [23]. DCs were pre-cultured at  $5 \times 10^4$  cell/cm $^2$  in a cell culture plate or a 35 mm glass-bottom dish with four chambers. Several hours later, InP-derived cancer vaccines prepared with F-OVA were added into DCs culture medium (5  $\mu$ g/mL of F-OVA and 25  $\mu$ g/mL of Fe-Ace complexes). Medium alone and medium supplemented with F-OVA at an equivalent dose served as controls. Following overnight coculture, DCs were stained with LysoTracker Red for lysosomes and Hoechst for nuclei. The samples were imaged with an SP5 confocal laser scanning microscope (CLSM, Leica) in the presence of ProLong Live Antifade Reagent. Furthermore, the harvested DCs were subjected to flow cytometry using an SP6800 Spectral Cell Analyzer (Sony). FlowJo v10 software was used to analyze the data.

**2.6. Proteolysis of DQ-OVA by DCs.** DCs were pre-cultured at  $1 \times 10^5$  cells/cm $^2$  in a cell culture plate or glass-bottom dish. Several hours later, InP-derived cancer vaccines prepared with DQ-OVA were added into DCs culture medium (5  $\mu$ g/mL of DQ-OVA and 25  $\mu$ g/mL of Fe-Ace complexes). DCs cocultured with medium alone and medium supplemented with an equivalent dose of free DQ-OVA served as controls. At the designated time (1 hour, 6 hours, 2 days, 3 days), DCs were harvested and subjected to flow cytometry analysis. In addition, one day later, DCs were mounted with SlowFade<sup>TM</sup> Diamond Antifade Mountant with DAPI and imaged with CLSM.

**2.7. *In vitro* DCs activation.** DCs with a density of  $2 \times 10^5$  cell/cm<sup>2</sup> were cocultured in cell culture plates with InP-derived cancer vaccines (5 µg/mL of OVA and 25 µg/mL of Fe-Ace complexes). Free OVA was used as a control. Three days later, DCs were harvested and blocked with anti-CD16/CD32 antibody. Subsequently, some DCs were incubated with anti-CD11c-APC, anti-CD86-APC/Cy7, anti-I-A/I-E (MHC II)-PE, and anti-CD197(CCR7)-PE/Cy7 antibodies (BioLegend). In addition, some DCs were incubated with anti-CD11c-FITC and anti-H-2K<sup>b</sup>-SIINFEKL-APC antibodies (BioLegend). Subsequently, flow cytometry was carried out.

**2.8. *In vivo* lymph node targeting.** C57BL/6J mice (female, 6 weeks old, CLEA Inc.) were administered subcutaneously with 100 µL per mouse of InP-derived cancer vaccines (100 µg F-OVA and 500 µg Fe-Ace complexes). Saline, F-OVA in free format, F-OVA + InP in free form served as controls. Approximately 16 hours later, the draining lymph nodes were harvested. After blocking, the cells were incubated with anti-CD11c-APC antibody (BioLegend). Subsequently, flow cytometry was carried out. Moreover, cryostat sections of lymph nodes were prepared using Tissue-Tek O.C.T. compound, mounted with SlowFade<sup>TM</sup> Diamond Antifade Mountant with DAPI and imaged with CLSM.

**2.9. *In vivo* DCs activation and antigen cross-presentation.** C57BL/6J mice were administered subcutaneously with 100 µL per mouse of InP-derived cancer vaccines (100 µg OVA and 500 µg Fe-Ace complexes). Saline, OVA in free format, OVA + InP in free form served as controls. Approximately 16 hours later, the draining lymph nodes were harvested. After blocking, the cells were incubated with anti-CD11c-APC, anti-CD197(CCR7)-PE/Cy7, anti-CD80-FITC, anti-CD86-APC/Cy7, and anti-H-2K<sup>b</sup>-SIINFEKL-PE antibodies (BioLegend). Subsequently, flow cytometry was carried out.

**2.10. *In vivo* tumor treatment experiments.** Thirty C57BL/6J mice were randomized into six groups. E.G7-OVA lymphoma cells at a dose of  $2 \times 10^5$  cells per mouse were injected subcutaneously into one side. After 4, 7, and 10 days, 100µL per mouse of the following samples were injected subcutaneously into the other side, respectively: 1) saline; 2) OVA (100 µg); 3) OVA + InP (100µg OVA and 500 µg InP); 4) Fe-Ace-O1 (OVA-encapsulated Fe-Ace coordination complexes); 5) Fe-Ace-O2 (OVA-encapsulated Fe-Ace coordination complexes synthesized in the presence of F127); 6) Fe-Ace-O3 (OVA-encapsulated Fe-Ace coordination complexes synthesized in the presence of PVP). The cancer vaccines (Fe-Ace-O1, Fe-Ace-O2 and Fe-Ace-O3) was all administered at a dose of 100 µg OVA and 500 µg Fe-Ace complexes per mouse. Tumors were measured periodically, and tumor volume was calculated as  $\text{length} \times \text{width}^2 / 2$ .

**2.11. Analysis of anti-tumor mechanism using flow cytometry.** At the endpoint, spleens and tumor-draining lymph nodes were harvested. Cell suspensions were prepared and blocked. Some splenocytes were incubated with anti-CD4-FITC and anti-CD8a-APC/Cy7 antibodies (Biolegend). Some splenocytes were incubated with anti-CD3-APC, anti-CD8a-APC/Cy7, and anti-T-Select H-2K<sup>b</sup> OVA Tetramer-SIINFEKL-PE (MBL) antibodies. Furthermore, the lymphocytes were incubated with anti-CD4-FITC, anti-CD8a-APC/Cy7, and anti-T-Select H-2K<sup>b</sup> OVA Tetramer-SIINFEKL-APC (MBL) antibodies. Subsequently, flow cytometry was carried out.

**2.12. Immunohistochemical, immunofluorescent, and conventional staining.** At the endpoint, the tumors were harvested and immersed in liquid nitrogen. Subsequently, the cryostat sections of the tumors were prepared

using Tissue-Tek O.C.T. compound. Some sections were treated with anti-Ki67 primary antibody and Rabbit specific HRP/DAB Detection IHC Detection Kit (abcam) to stain proliferating cells. Some sections were treated with TUNEL Assay Kit - HRP-DAB (abcam) to stain apoptosis. Some sections were treated with hematoxylin and eosin (H&E). All sections were then imaged under a light microscope (DMIL, Leica). In addition, some sections were incubated with anti-CD80-FITC antibody (Biolegend) for M1 macrophages, mounted with SlowFade™ Diamond Antifade Mountant with DAPI and imaged with CLSM.

**2.13. *Ex vivo* analysis.** At the endpoint, the lymph nodes of mice administered with cancer vaccines Fe-Ace-O2 were harvested. Then, the cells were incubated with either OVA antigen or Lewis lung carcinoma (LLC) cell lysates for several hours. After blocking, the cells were incubated with anti-CD3-APC, anti-CD8a-APC/Cy7, and anti-IFN- $\gamma$ -PE antibodies (Biolegend). Subsequently, flow cytometry was carried out.

**2.14. Enzyme-linked immunosorbent assay (ELISA).** At the endpoint, the spleens were homogenized using a tissue protein extraction reagent (Thermo Scientific Inc.), and cytokines were measured using ELISA kits (BD Biosciences).

**2.15. CD8<sup>+</sup> T cells depletion.** To determine whether the antitumor immune response is dependent on CD8<sup>+</sup> T cells, E.G7-OVA lymphoma cells were injected subcutaneously into one side of mice. After 4, 7, and 10 days, Fe-Ace-O2 suspensions were administered subcutaneously into the other side, along with intraperitoneal injection of Ultra-LEAF™ purified anti-mouse CD8a antibody (200  $\mu$ g/mouse, Biolegend) each time. Mice subcutaneously injected with self-assembled cancer vaccines only or 100 $\mu$ L saline only were used as controls. Tumors were measured regularly.

**2.16. *In vivo* biocompatibility test.** To assess *in vivo* safety, the samples were administered subcutaneously C57BL/6J mice at a dose of 1 mg / 100 $\mu$ L saline per mouse. OVA group and OVA+InP group with equivalent OVA or InP, and saline group were served as controls. 3 days later, mice were euthanized. Blood samples were taken for biochemical analysis.

**2.17. Statistical Analysis.** Data were analyzed by one-way analysis of variance (ANOVA) with Tukey's *post hoc* test for multiple comparisons. Statistical significance was defined as  $p \leq 0.05$ . All results were shown as mean  $\pm$  standard deviation (SD).

**2.18. Ethical approval.** Prior to initiating the animal studies, approval was granted by the Animal Experimentation Committee of the National Institute for Materials Science (NIMS) in Japan.

### 3. Results

**3.1. Characterization of Fe-Ace coordination complexes and self-assembled cancer vaccines.** Fe-Ace coordination complexes were synthesized (Table 1). The morphological analysis was carried out using scanning electron microscopy (SEM). Fe-Ace coordination complexes (Fe-Ace-a and Fe-Ace-b), synthesized at room temperature using FeCl<sub>3</sub>·6H<sub>2</sub>O and InP in the final ratio of 20 mM:9 mM and 40 mM:9 mM, exhibit fibrous morphology with lengths of 50  $\mu$ m and 20  $\mu$ m, respectively (Figure 1a, A, B). When synthesized in an ice bath using FeCl<sub>3</sub>·6H<sub>2</sub>O and InP in the ratio of 40 mM:9 mM, the obtained Fe-Ace coordination complexes (Fe-Ace-



1) exhibit a reduction in particle size, with a length of approximately 4  $\mu\text{m}$  (Figure 1a, C). Considering the shorter length of Fe-Ace-1, subsequent experiments were carried out based on this synthesis parameter. In addition, Fe-Ace coordination complexes synthesized with the addition of surfactants F127 and PVP were designated as Fe-Ace-2 and Fe-Ace-3, respectively.

**Table 1.** Typical synthesis parameters for Fe-Ace coordination complexes

	$\text{FeCl}_3 \cdot 6\text{H}_2\text{O}$	InP	F127	PVP	mark
Fe-Ace-a	20 mM	9 mM	-	-	RT
Fe-Ace-b	40 mM	9 mM	-	-	RT
Fe-Ace-1	40 mM	9 mM	-	-	Ice bath
Fe-Ace-2	40 mM	9 mM	1.6 mg/mL	-	Ice bath
Fe-Ace-3	40 mM	9 mM	-	4 mg/mL	Ice bath

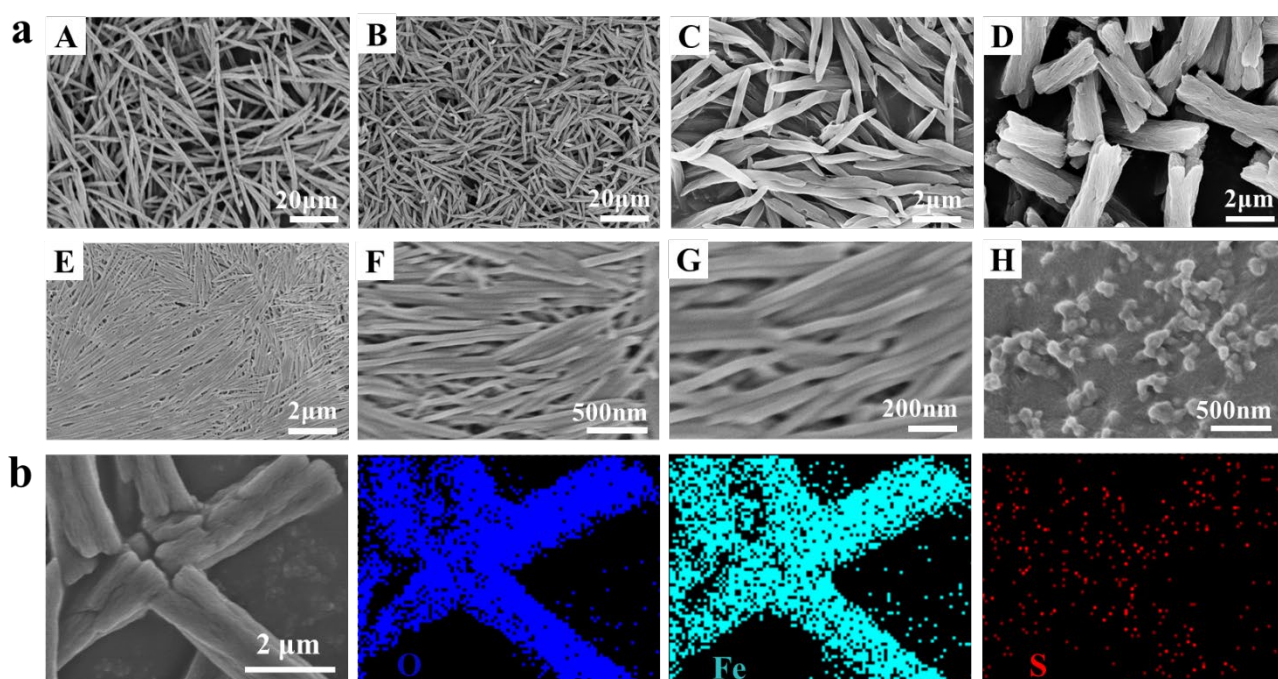


**Figure. 1** Fe-Ace coordination complexes and self-assembled cancer vaccines with tailored morphology and particle size. (a) SEM images of Fe-Ace coordination complexes (A, Fe-Ace-a; B, Fe-Ace-b; C, Fe-Ace-1) and self-assembled vaccines (D, Fe-Ace-O1; E, F, G, Fe-Ace-O2; H, Fe-Ace-O3). (b) EDX mapping analysis (Fe, O and S elements) of self-assembled vaccines Fe-Ace-O1 based on Fe-Ace coordination complexes.

To prepare InP-derived self-assembled cancer vaccines, OVA model antigen was encapsulated into Fe-Ace coordination complexes during the synthesis process. The resulting self-assembled cancer vaccines range from microscale to nanoscale, with shapes including rods, fibers, and spheres, by simply tuning the synthesis parameters (temperature, concentration of raw materials, and so on), and the type of surfactant. Self-assembled cancer vaccines synthesized in water, F127-containing aqueous solution, and PVP-containing aqueous solution were named Fe-Ace-O1, Fe-Ace-O2, and Fe-Ace-O3, respectively. Self-assembled cancer vaccines Fe-Ace-O1, synthesized using  $\text{FeCl}_3 \cdot 6\text{H}_2\text{O}$  and InP in the final ratio of 40 mM:9 mM in the presence of 2 mg/mL OVA in an ice bath, exhibit bone-like rod morphology with the width of about 1.5  $\mu\text{m}$  and the length of about 4  $\mu\text{m}$

(Figure 1a, D). A comparison of the morphology of Fe-Ace-O1 and Fe-Ace-1 suggests that in the absence of surfactant, the addition of OVA results in an increase in the width of the formed particles without a change in the length. EDX mapping characterization of self-assembled vaccines Fe-Ace-O1 reveals that model tumor antigen OVA containing S elements is homogeneously and efficiently embedded in the simultaneously formed Fe-Ace coordination complexes at the nanoscale (Figure 1b). Upon the addition of F127 into the synthesis solution, self-assembled cancer vaccines Fe-Ace-O2 exhibit nanofibrous morphology with a width of about 40 nm and a length of 0.5 ~ 3  $\mu\text{m}$  (Figure 1a, E-G). The addition of PVP in the synthesis solution results in the formation of self-assembled cancer vaccines Fe-Ace-O3 with nanospherical morphology and an average diameter of 50 ~ 80 nm (Figure 1a, H). The present self-assembled cancer vaccines can be dispersed well for several hours and easily injected using syringe with 26G needle.

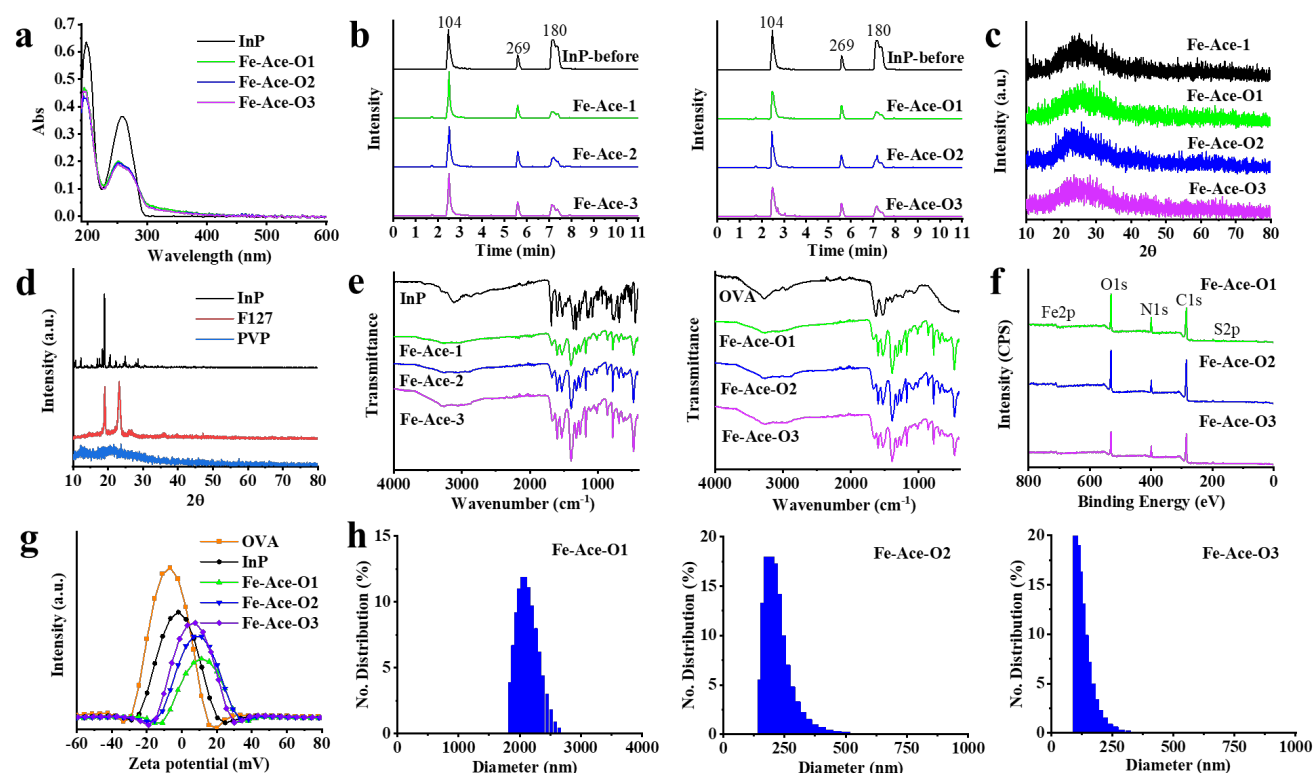


**Figure. 2** Physicochemical properties of Fe-Ace coordination complexes and self-assembled cancer vaccines. (a) UV-vis spectra of InP aqueous solution equivalent to the reaction solution and supernatant solution after reaction (Fe-Ace-O1, Fe-Ace-O2, Fe-Ace-O3); (b) HPLC-MS spectra of InP aqueous solution equivalent to the reaction solution and supernatant solution after reaction; (c, d) XRD patterns of samples and raw materials; (e) FTIR spectra of samples; (f) XPS spectra of samples; (g) Zeta potentials of samples; (h) Particle size distribution of samples

UV-vis absorption spectra of InP aqueous solution equivalent to the reaction solution and supernatant solution after the reaction are shown in **Figure 2a**. The initial InP aqueous solution shows a peak at 260 nm, and the absorbance of supernatant after the reaction at 260 nm decreased to the same extent for all the self-assembled vaccines (Fe-Ace-O1, O2, O3). InP aqueous solution and supernatant solution after reaction were further analyzed using HPLC-MS (Figure 2b). In the initial InP aqueous solution, three peaks with mass-to-charge ratio ( $m/z$ ) of 104, 269 and 180 with retention time of 2.5 min, 5.6 min and 7.2 min, respectively, are observed,



representing dimethylaminoisopropanol, inosine and acedoben, respectively. In the supernatant after the reaction, the concentrations of dimethylaminoisopropanol and inosine do not change significantly, but the concentration of acedoben decreases significantly. The reaction efficiencies of acedoben for Fe-Ace coordination complexes (Fe-Ace-1, 2, 3) and self-assembled vaccines (Fe-Ace-O1, O2, O3) are about 80%. The loading efficiencies of OVA for self-assembled vaccines (Fe-Ace-O1, O2, O3) are about 50%.

XRD patterns of the self-assembled cancer vaccines exhibit a broad peak around  $20^{\circ}\sim 30^{\circ}$ , indicating their amorphous phases (Figure 2c), while the raw materials InP and F127 demonstrate a crystalline state (Figure 2d). The results of FTIR analysis indicate the synthesis of Fe-Ace coordination complexes (Figure 2e). With regard to InP, a distinct C=O stretching band is apparent at  $1684\text{ cm}^{-1}$ , corresponding to the carboxylic acid groups in acedoben. In contrast, in Fe-Ace-1, 2, 3 and Fe-Ace-O1, O2, O3, weak C=O stretching bands near  $1670\text{ cm}^{-1}$  are observed, indicative of the presence of metal carboxylates. XPS further reveals the synthesis of Fe-Ace coordination complexes (Figure 2f).

The zeta potential of OVA and InP in saline is centered at  $-7.2\text{ mV}$  and  $-2.3\text{ mV}$ , respectively, whereas those of Fe-Ace-O1, Fe-Ace-O2 and Fe-Ace-O3 in saline are around  $+11.5\text{ mV}$ ,  $+9.1\text{ mV}$  and  $+6.4\text{ mV}$ , respectively (Figure 2g). The hydrodynamic sizes of Fe-Ace-O1, Fe-Ace-O2 and Fe-Ace-O3 are  $2\text{ }\mu\text{m}$ ,  $200\text{ nm}$  and  $100\text{ nm}$ , respectively, as determined by DLS analysis (Figure 2h). The DLS results for Fe-Ace-O1 and Fe-Ace-O2 are different from the SEM images due to their rod and fibrous structures. Moreover, sonication prior to testing may result in the shortening of the nanofibrous structure of the Fe-Ace-O2 sample.

**3.2. Effects of the morphology of self-assembled cancer vaccines on antigen uptake, proteolysis and DCs activation *in vitro*.** DCs represent the most professional APCs within the body, which are responsible for capturing and processing antigen, presenting them to T cells in the lymph node, and initiating an adaptive immune response. Therefore, primary DCs were employed in the study to evaluate the cellular uptake of OVA antigens *in vitro*.

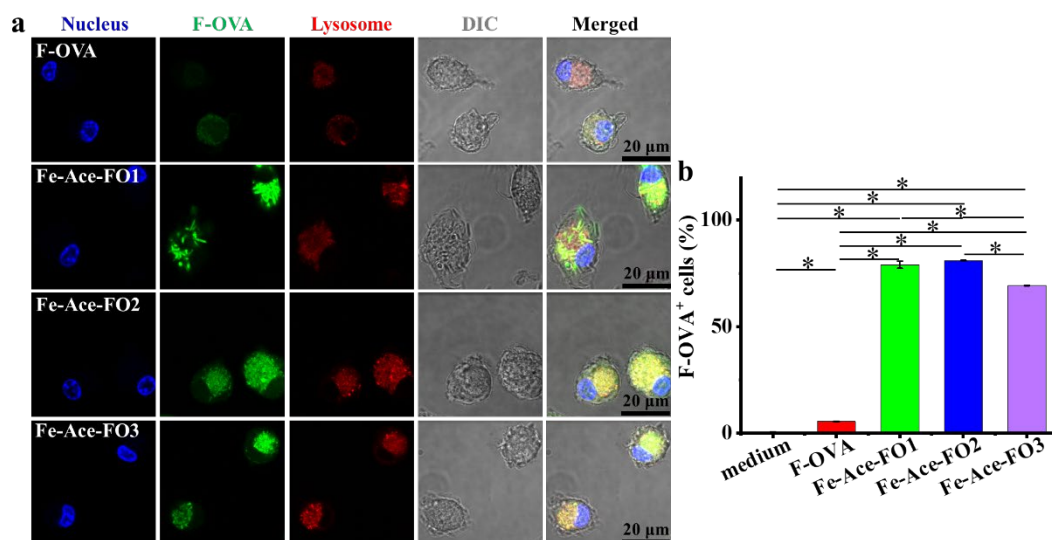


**Figure. 3** Self-assembled cancer vaccines enhance F-OVA antigen uptake by DCs. (a) Representative CLSM images of DCs after overnight coculture with F-OVA or self-assembled cancer vaccines (Fe-Ace-FO1, Fe-Ace-FO2 and Fe-Ace-FO3). (b) Quantitative analysis of F-OVA uptake by DCs (n=3, \*  $p<0.05$ ).

To visualize the antigens, the green fluorescent F-OVA upon excitation was employed to synthesize self-

assembled cancer vaccines (Fe-Ace-FO1, Fe-Ace-FO2, Fe-Ace-FO3). As a control, F-OVA was used. As shown in **Figure 3a**, the Fe-Ace-FO1, Fe-Ace-FO2 and Fe-Ace-FO3 groups have significantly higher fluorescence signals than the free F-OVA group, suggesting that F-OVA biomolecules encapsulated in self-assembled cancer vaccines are more efficiently taken up by DCs than free F-OVA. Moreover, self-assembled cancer vaccines are localized around the nucleus and entrapped partly inside lysosomal compartment of DCs due to the partial overlap of the green fluorescence of F-OVA and the red fluorescence of lysosomes. Quantitative analysis results further suggest all the self-assembled cancer vaccines groups exhibit much higher F-OVA cellular uptake by DCs than free group (Figure 3b). In addition, Fe-Ace-FO1 and Fe-Ace-FO2 groups show higher F-OVA uptake than Fe-Ace-FO3 group, suggesting that PVP surface modification may affect the uptake of particles by DCs.

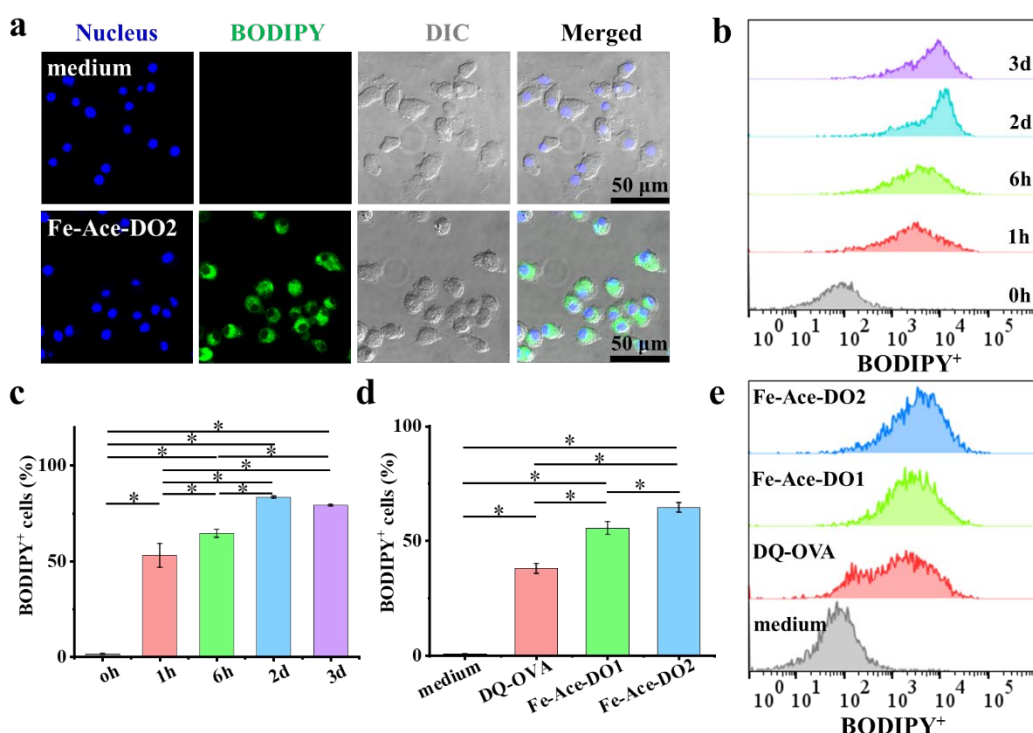


**Figure. 4** Proteolysis of model antigen DQ-OVA in self-assembled cancer vaccines following uptake by DCs *in vitro*. (a) Representative CLSM images of DCs after overnight coculture with self-assembled vaccines (Fe-Ace-DO2). DCs cocultured with medium are used as control. (b, c) Representative histograms (b) and quantitative analysis (c) of DQ-OVA hydrolysis (BODIPY<sup>+</sup> cell populations) after culturing DCs with self-assembled vaccines (Fe-Ace-DO2) for different times (1h, 6h, 2d, 3d). (d, e) Quantitative analysis (d) and representative histograms (e) of DQ-OVA hydrolysis (BODIPY<sup>+</sup> cell populations) after culturing DCs with medium, free DQ-OVA and self-assembled vaccines (Fe-Ace-DO1, Fe-Ace-DO2) after 6 hours. Data in c-d, n=3, \* p<0.05.

To visualize the proteolysis process of the antigens, DQ ovalbumin (DQ-OVA) was used to prepare self-assembled cancer vaccines synthesized in water and F127-containing aqueous solution, which were named Fe-Ace-DO1 and Fe-Ace-DO2, respectively. Only culture medium and an equivalent dose of free DQ-OVA were used as controls. For DQ-OVA, OVA antigen proteins are heavily labeled with BODIPY dyes, resulting in a strong fluorescence quenching effect. When DQ-OVA is proteolytically hydrolyzed into a single, dye-labeled peptide, this quenching phenomenon is relieved and bright green fluorescence is presented. As shown in **Figure**

4a-c, coculture of self-assembled vaccines (Fe-Ace-DO2) with DCs results in the uptake of the particles and subsequent proteolytic degradation of DQ-OVA embedded in the particles. From the initial point to two days, the intensity of green fluorescence exhibits a gradual increase over time, reaching a plateau and subsequently declining. In comparison to free DQ-OVA and self-assembled vaccines Fe-Ace-DO1, self-assembled vaccines Fe-Ace-DO2 exhibit a stronger green fluorescence after 6 hours (**Figure 4d-e**).

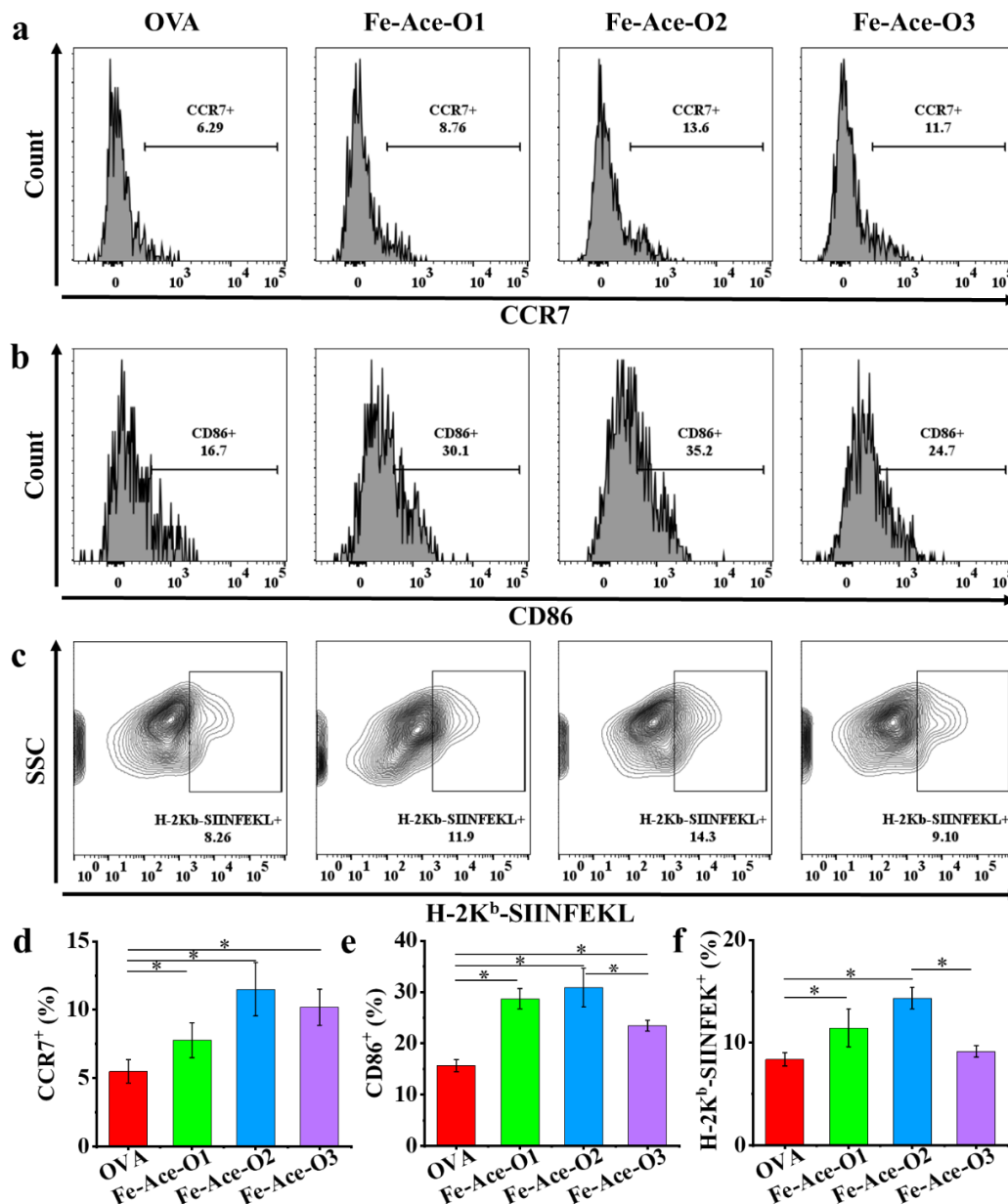


**Figure. 5** Nanofibrous self-assembled cancer vaccines effectively enhance DCs activation and antigen cross-presentation *in vitro*. (a-c) Representative histograms of DCs cell markers (a, CCR7<sup>+</sup> in CD11c<sup>+</sup>; b, CD86<sup>+</sup> in CD11c<sup>+</sup>MHC II<sup>+</sup>; c, H-2Kb-SIINFEKL<sup>+</sup> in CD11c<sup>+</sup>) after coculture for 3 days. (d-f) Quantitative analysis of DCs activation and antigen cross-presentation after coculture for 3 days. Data in d-f, n=3, \* p<0.05.

Furthermore, when DCs were cocultured with self-assembled cancer vaccines for 3 days, their activation and antigen cross-presentation were assessed by flow cytometry (**Figure 5**). The Fe-Ace-O1, Fe-Ace-O2 and Fe-

Ace-O3 groups have significantly higher CCR7<sup>+</sup>, CD86<sup>+</sup> and H-2K<sup>b</sup>-SIINFEKL<sup>+</sup> cell populations than those cocultured with free OVA. Moreover, DCs cocultured with nanofibrous self-assembled cancer vaccines Fe-Ace-O2 show higher CCR7<sup>+</sup>, CD86<sup>+</sup> and H-2K<sup>b</sup>-SIINFEKL<sup>+</sup> cell populations than those cocultured with microscale self-assembled cancer vaccines Fe-Ace-O1 and spherical self-assembled cancer vaccines Fe-Ace-O3.

**3.3. Nanofibrous self-assembled vaccines significantly improve targeted lymph node delivery and *in vivo* cross-presentation of tumor antigens.** Self-assembled vaccines groups and free F-OVA group exhibit green fluorescence intensity in lymph nodes in the order of Fe-Ace-FO2 > Fe-Ace-FO3 > Fe-Ace-FO1, free F-OVA (**Figure 6**). The images suggest that nanoscale Fe-Ace-FO2 and Fe-Ace-FO3 exhibit much stronger targeted lymph node delivery than microscale Fe-Ace-FO1. Meanwhile, nanofibrous Fe-Ace-FO2 shows a stronger targeted lymph node delivery than nanospherical Fe-Ace-FO3.

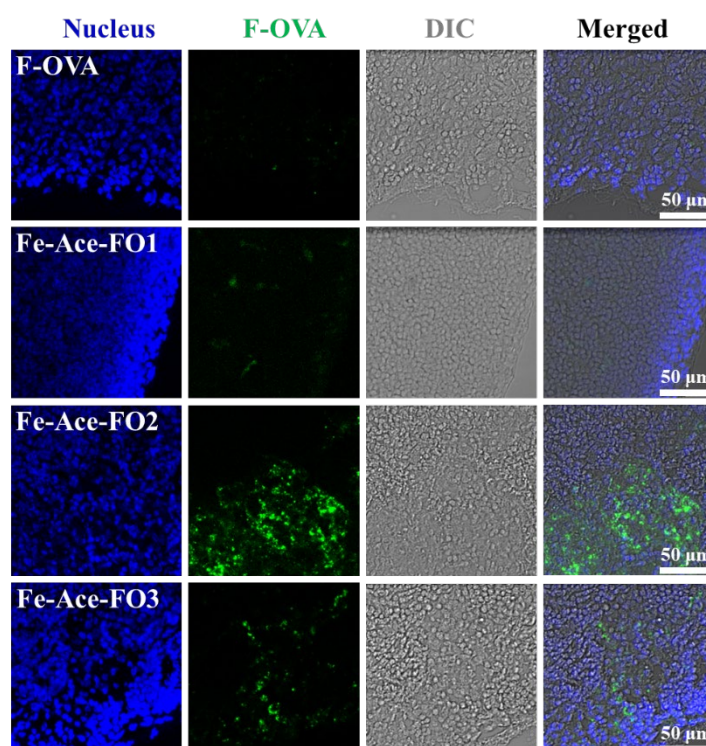


**Figure. 6** *In vivo* targeted lymph node delivery of F-OVA tumor antigens. Representative CLSM images for free F-OVA and self-assembled vaccines (Fe-Ace-FO1, Fe-Ace-FO2 and Fe-Ace-FO3).

Afterwards, targeted lymph node delivery, DCs activation and antigen cross-presentation *in vivo* were quantified by F-OVA<sup>+</sup> in CD11c<sup>+</sup>, CCR7<sup>+</sup> in CD11c<sup>+</sup>, CD80<sup>+</sup>CD86<sup>+</sup> in CD11c<sup>+</sup>, and H-2K<sup>b</sup>-SIINFEKL<sup>+</sup> in CD11c<sup>+</sup> (**Figure 7**). In this study, the cell populations of F-OVA<sup>+</sup> in CD11c<sup>+</sup> in lymph nodes represent those of DCs that have captured model antigens F-OVA embedded in self-assembled vaccines or in free format and then migrate to lymph nodes. As shown in **Figure 7a, b**, flow cytometry analysis results are consistent with the CLSM images mentioned in Figure 6. The cell population of F-OVA<sup>+</sup> in CD11c<sup>+</sup> in lymph node for nanofibrous self-assembled vaccines Fe-Ace-FO2 is 7.89±0.33%, which is much higher than those for free F-OVA group (2.05±0.33%), free F-OVA+InP group (3.32±0.10%), microscale self-assembled vaccines Fe-Ace-FO1 (1.28±0.67%) and nanospherical self-assembled vaccines Fe-Ace-FO3 (5.94±0.66%).



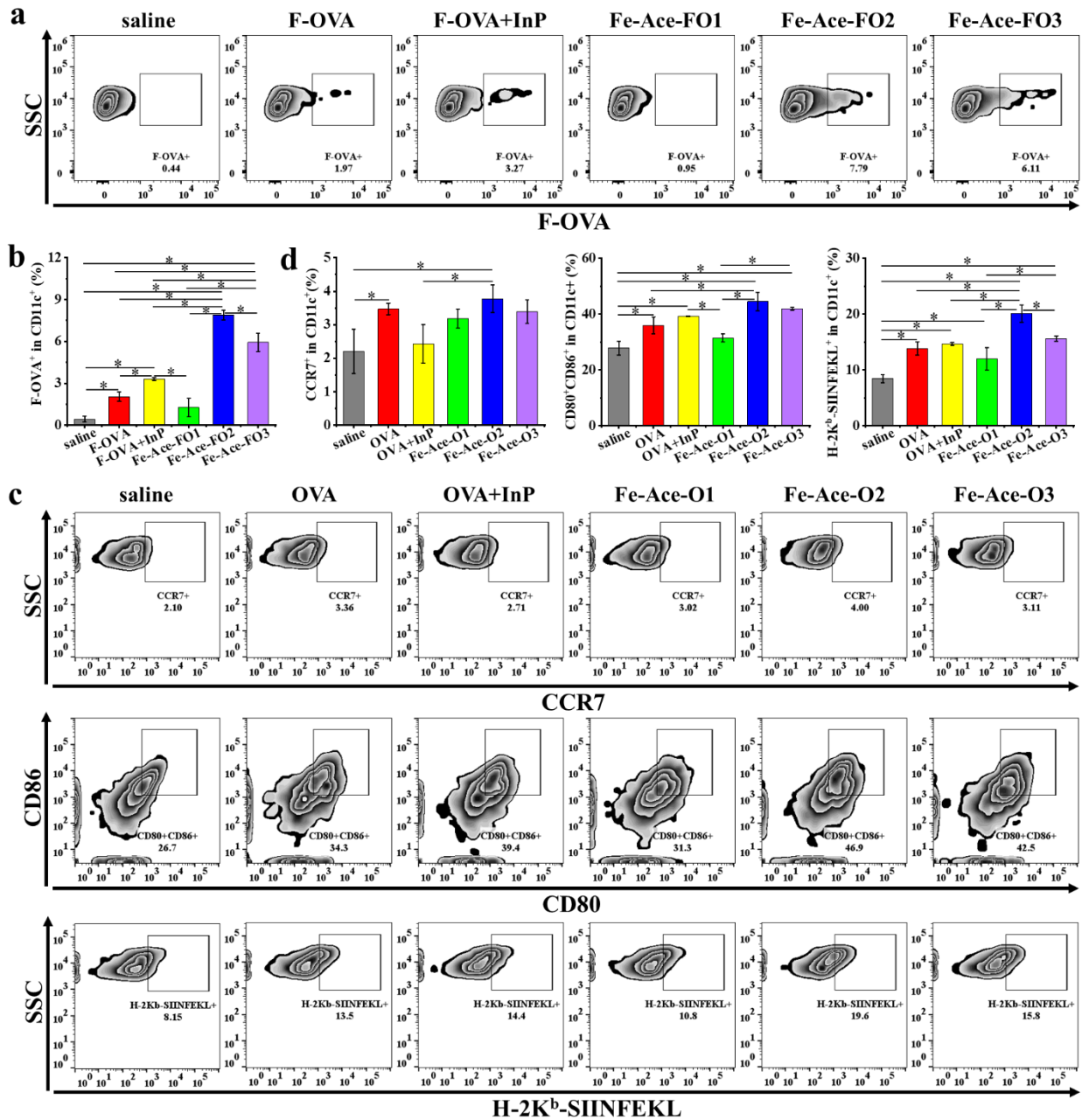


**Figure. 7** Nanofibrous self-assembled vaccines significantly enhance targeted lymph node delivery, DCs activation and antigen cross-presentation *in vivo*. (a, b) Representative plots and quantitative analysis of F-OVA<sup>+</sup> in CD11c<sup>+</sup>. (c, d) Representative plots and quantitative analysis of CCR7<sup>+</sup> in CD11c<sup>+</sup>, CD80<sup>+</sup>CD86<sup>+</sup> in CD11c<sup>+</sup>, and H-2K<sup>b</sup>-SIINFEKL<sup>+</sup> in CD11c<sup>+</sup>. Data in b, d, n=3, \* p<0.05.

Nanofibrous self-assembled vaccines Fe-Ace-O2 show higher percentages of CCR7<sup>+</sup> in CD11c<sup>+</sup> in lymph nodes than other groups, which suggests the homing of DCs from the peripheral tissues to lymphoid organs as mentioned above (Figure 7c, d). Moreover, nanofibrous self-assembled vaccines Fe-Ace-O2 facilitate the increase in the percentages of CD80<sup>+</sup>CD86<sup>+</sup> in CD11c<sup>+</sup> in lymph nodes, which represents the activation of DCs. Most importantly, nanofibrous self-assembled vaccines Fe-Ace-O2 are more efficient than others in enhancing *in vivo* antigen cross-presentation.

**3.4. Inhibitory effects of self-assembled vaccines on tumors at the distant site.** Antitumor efficacy of self-assembled vaccines was evaluated (**Figure 8**). Mice treated with OVA in free format (free OVA group) exhibit comparable tumor growth curves with those without any treatment (saline group). This suggests that only tumor antigen OVA at the dose of 100  $\mu\text{g}/\text{mouse}$  without the addition of adjuvants and carriers is not able to generate an effective antitumor immunity to inhibit the tumor growth. The mixture of OVA and InP in free format (free OVA + InP group) inhibits the tumor growth to some extent, compared with saline and free OVA groups, indicating the adjuvant function of InP drug. Further, mice treated with microscale self-assembled vaccines Fe-Ace-O1 and nanofibrous self-assembled vaccines Fe-Ace-O2 more effectively inhibit tumor growth than free OVA + InP group, since Fe-Ace coordination complexes simultaneously act as adjuvants and carriers for tumor antigens. In addition, mice treated with nanospherical self-assembled vaccines Fe-Ace-O3 show comparable antitumor efficacy with free OVA + InP group, which is weaker than other self-assembled vaccines Fe-Ace-O1 and Fe-Ace-O2. Among all the groups, nanofibrous self-assembled vaccines Fe-Ace-O2 exhibit the strongest effects on the inhibition of tumor growth.

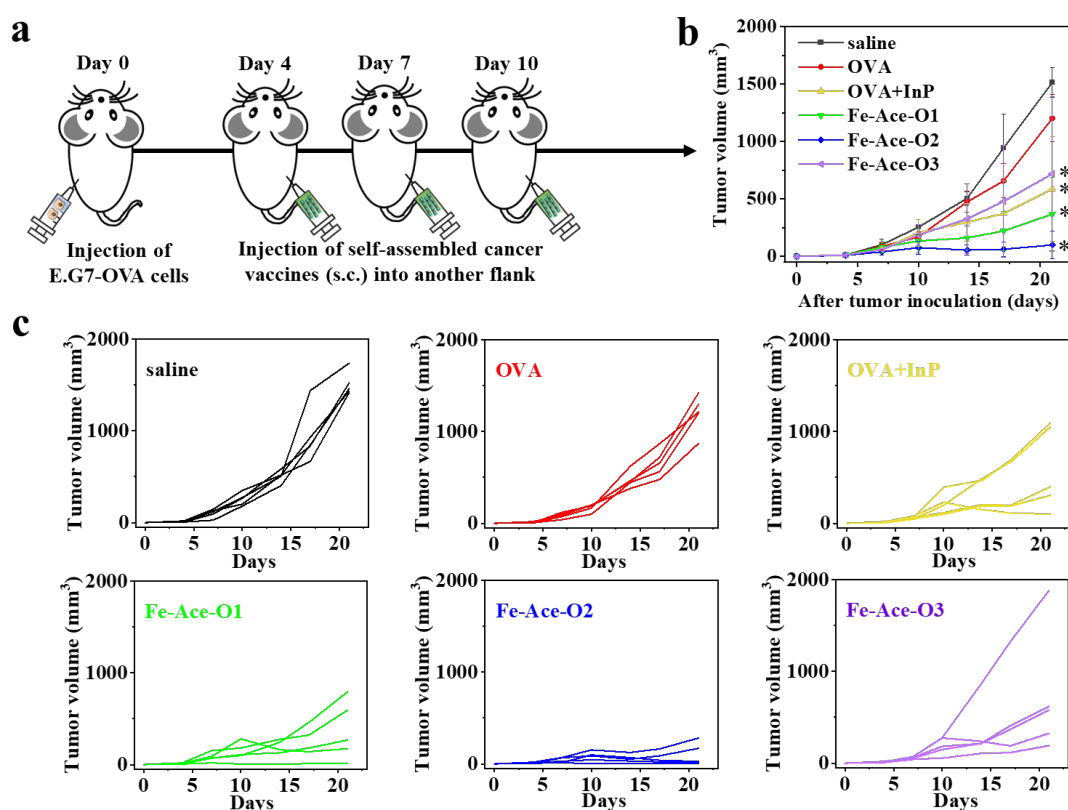


**Figure. 8** Inhibitory effects of self-assembled vaccines on tumors at the distant site. (a) Schematic diagram of antitumor tests. (b) Average tumor growth curves. Data in b,  $n=5$ , \*  $p<0.05$ . (c) Individual tumor growth curves.

**3.5. Antitumor immune mechanism research underlying self-assembled cancer vaccines.** To explore the underlying mechanism of the antitumor therapeutic efficacy among different groups, the spleen and lymph nodes were used to quantify the percentages of  $\text{CD4}^+$ ,  $\text{CD8}^+$ , tetramer<sup>+</sup> in  $\text{CD3}^+\text{CD8}^+$ , tetramer<sup>+</sup> $\text{CD8}^+$  T cells (**Figures 9, 10**). The percentages of  $\text{CD4}^+$  or  $\text{CD8}^+$  T cells in spleen of free OVA + InP group and self-assembled vaccines groups (Fe-Ace-O1, Fe-Ace-O2, Fe-Ace-O3) are significantly higher than those of free OVA group (Figure 9 a-c). The average percentages of tetramer<sup>+</sup> in  $\text{CD3}^+\text{CD8}^+$  T cells in splenocytes of nanofibrous self-



assembled vaccines group (Fe-Ace-O2) are much higher than other groups (Figure 9 d, e). For nanofibrous self-assembled vaccines Fe-Ace-O2, the percentages of  $CD4^+$ ,  $CD8^+$  or tetramer $^+$  $CD8^+$  T cells in lymphocytes are significantly higher than free OVA + InP group, microscale self-assembled vaccines Fe-Ace-O1 and nanospherical self-assembled vaccines Fe-Ace-O3 (Figure 10).

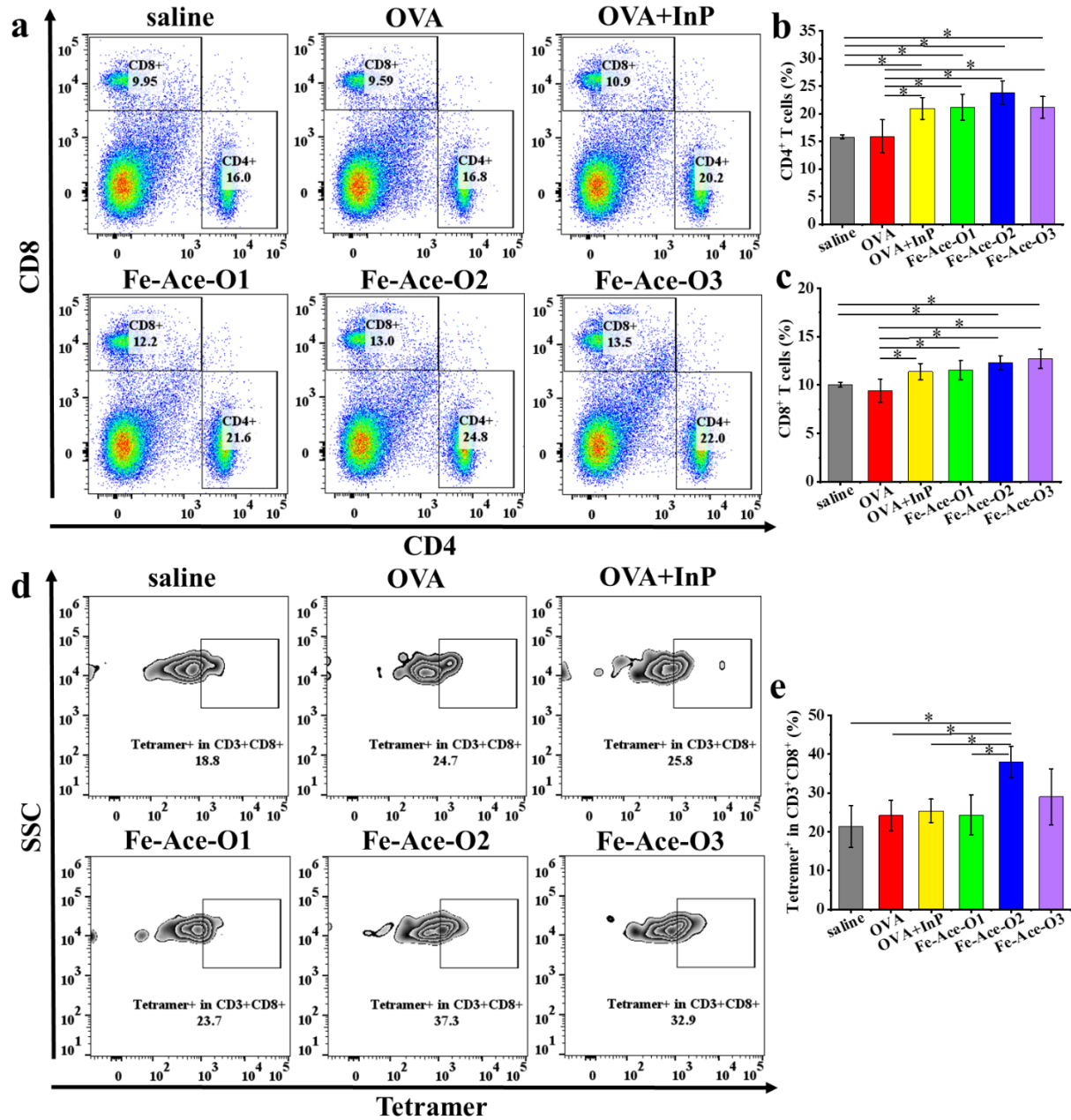


**Figure. 9** Analysis of antitumor mechanism using splenocytes. (a-e) Representative plots and quantitative results:  $CD4^+$  and  $CD8^+$  T cells (a-c); tetramer $^+$  in  $CD3^+$  $CD8^+$  T cells (d, e). Data in b-c, e, n=5, \* p<0.05.

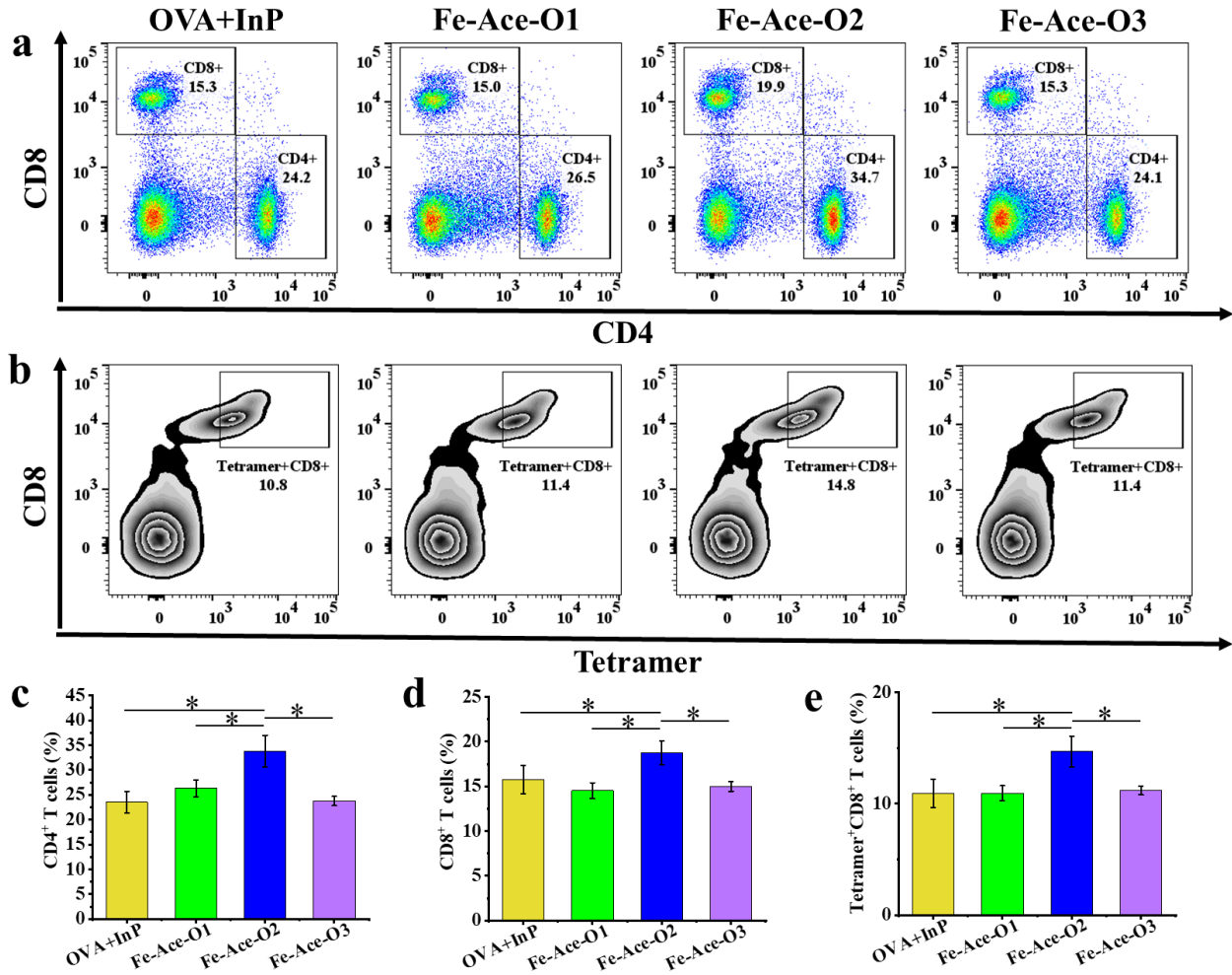


**Figure. 10** Analysis of antitumor mechanism using lymphocytes. (a-e) Representative plots and quantitative results: CD4<sup>+</sup> (a, c), CD8<sup>+</sup> (a, d) and tetramer<sup>+</sup>CD8<sup>+</sup> (b, e) T cells. Data in c-e, n=5, \* p<0.05.

Immunohistochemical, immunofluorescent, and conventional staining of tumor cryosections was carried out to further analyze the antitumor mechanism (**Figure 11**). Immunohistochemical staining of the sections using anti-Ki67 antibody shows that the highly proliferative tumor cells were much less in nanofibrous self-assembled vaccines group (Fe-Ace-O2) than other five groups (Figure 11 a). TUNEL staining of tumor sections exhibits higher levels of apoptosis in Fe-Ace-O2 group than other groups (Figure 11 b). H&E staining of tumor sections indicates large necrosis regions in Fe-Ace-O2 group, compared with other groups (Figure 11 c). Moreover, immunofluorescent staining of immunostimulating M1 macrophages shows stronger green fluorescence in Fe-Ace-O2 group than other groups (Figure 11 d).

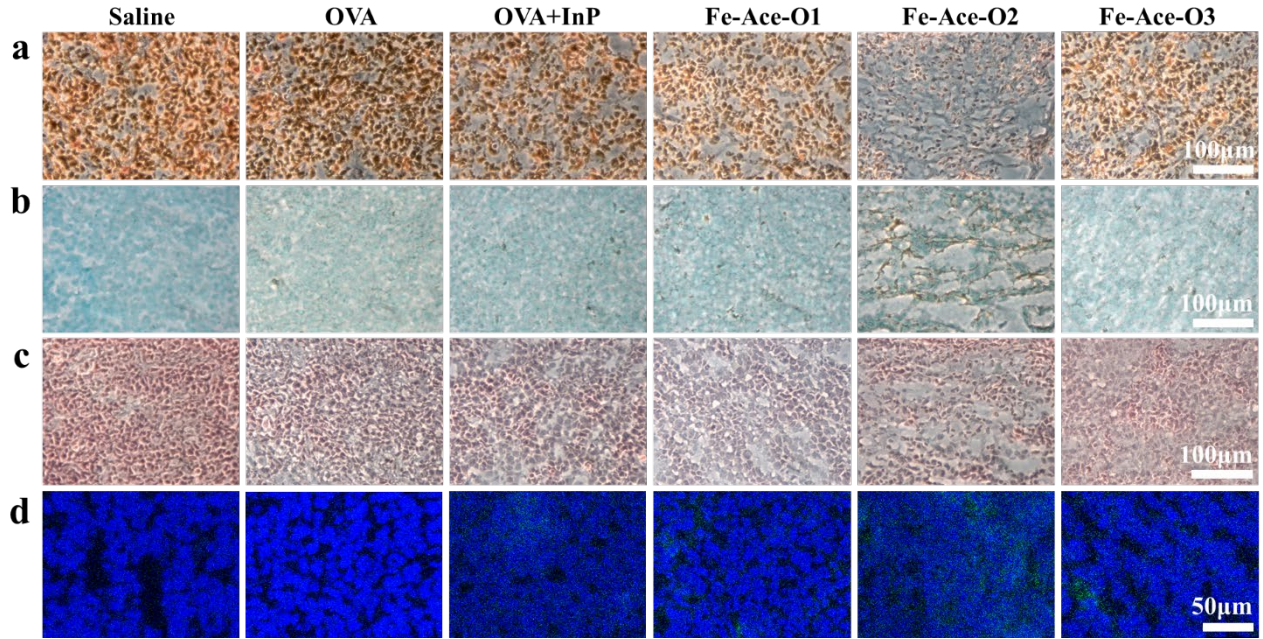


**Figure. 11** Analysis of antitumor mechanism using tumor sections. (a-d) Images of sections stained with anti-Ki67 antibody (a), TUNEL assay kit (b), H&E (c), and anti-CD80-FITC antibody and DAPI (d).

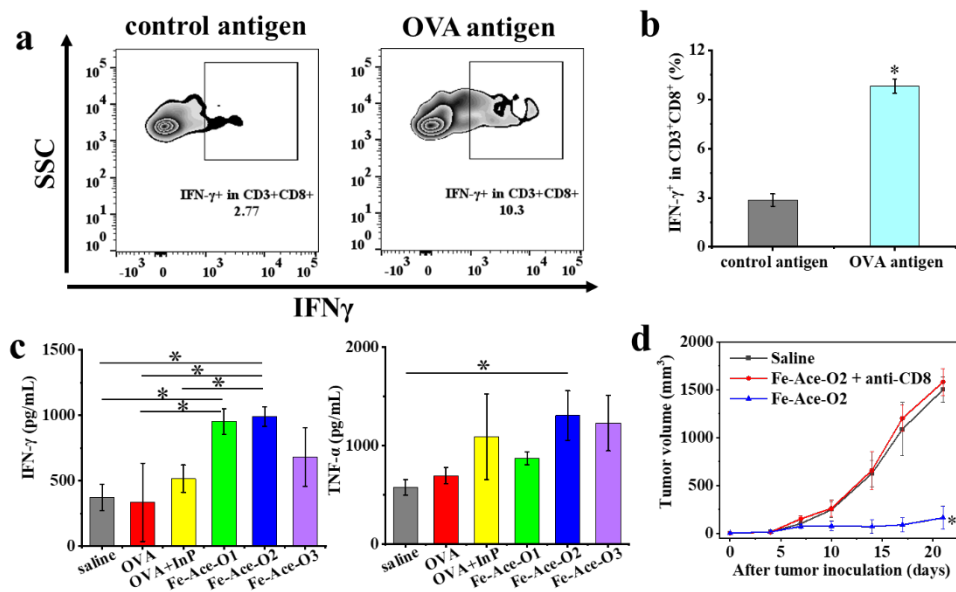


**Figure. 12** Analysis of antitumor mechanism. (a, b) Representative plots (a) and populations (b) of IFN- $\gamma^+$  in CD3 $^+$ CD8 $^+$  T cells in lymphocytes of mice treated with nanofibrous self-assembled vaccines Fe-Ace-O2 after stimulated by OVA antigen or LLC cell lysate (control antigen). Data in b, n=4, \* p<0.05. (c) Quantitative analysis of cytokines in spleen (n=3, \* p<0.05). (d) Tumor growth curves of mice treated with nanofibrous self-assembled vaccines Fe-Ace-O2 and T cell depletion. Mice treated with saline alone and nanofibrous self-assembled vaccines Fe-Ace-O2 alone were used as controls (n=5, \* p<0.05).

The lymphocytes of mice treated with nanofibrous self-assembled vaccines Fe-Ace-O2, stimulated with OVA model antigen for 2 hours, exhibit high percentage of IFN- $\gamma^+$  in CD3 $^+$ CD8 $^+$  T cells, compared with those stimulated with irrelevant control antigen from LLC cell lysates (**Figure 12 a, b**). The results confirm that T

cells in the lymph node of mice treated with self-assembled cancer vaccines can recognize OVA antigen.

Spleen cytokine levels are shown in **Figure 12 c**. Mice treated with nanofibrous self-assembled vaccines Fe-Ace-O2 have significantly higher IFN- $\gamma$  levels than saline, free OVA, free OVA + InP, and microscale self-assembled vaccines Fe-Ace-O1. Moreover, nanofibrous self-assembled vaccines show significantly higher TNF- $\alpha$  levels than saline.

To further confirm whether the antitumor immunity induced by self-assembled vaccines was dependent on CD8<sup>+</sup> T cells, intraperitoneal injection of anti-mouse CD8a antibody was performed to deplete CD8<sup>+</sup> T cells and the antitumor efficacy was evaluated. The results showed that the depletion of CD8<sup>+</sup> T cells resulted in rapid tumor growth (**Figure 12 d**).

**3.6. Blood biochemical analysis.** Blood biochemical analysis was performed three days after subcutaneous injection of 1 mg self-assembled vaccine into C57Bl/6J mice (**Figure 13**). Various biochemistry parameters, including blood urea nitrogen (BUN), creatinine (CRE), alanine aminotransferase (ALT), aspartate aminotransferase (AST), and alkaline phosphatase (ALP), were analyzed in this study. For the self-assembled vaccine group, the kidney function markers (BUN, CRE) and the liver function markers (ALT, AST, ALP) are all within the normal range as compared with those for saline, indicating no obvious hepatic or renal toxicity.

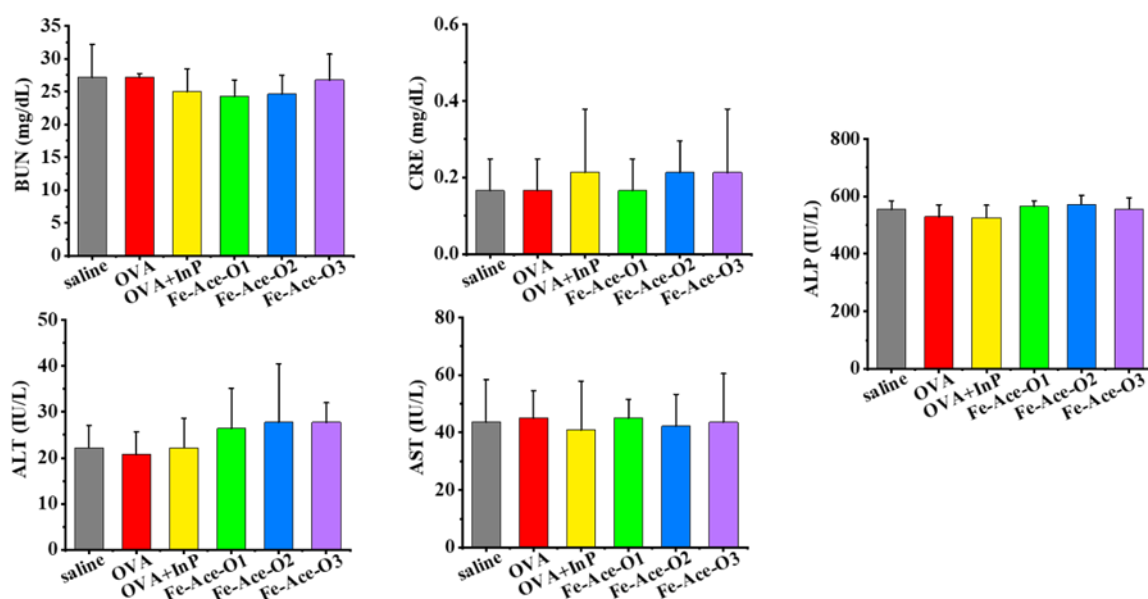


**Figure. 13** *In vivo* biocompatibility analysis. Blood biochemical analysis results 3 days after subcutaneous injection of self-assembled cancer vaccines (1 mg/mouse). OVA group and OVA+InP group with equivalent OVA or InP, and saline group were used as controls. Data in b, n=3.

#### 4. Discussion

Recently, self-assembled vaccines have attracted increasing attention in cancer immunotherapy [24-26]. For example, two potential adjuvants, toll-like receptor (TLR) 4 agonist (monophosphatidyl A, MPLA) and TLR9 agonist (CpG-ODN), were conjugated to encapsulate tumor antigen and prepare carrier-free self-assembled vaccines [24]. TLR7/8 agonist-epitope conjugate was developed to prepare self-assembled vaccines [25]. Cyclic-dinucleotide (CDN) STING agonists and manganese ions were reported to self-assemble into nanoparticles and exhibit robust anti-tumor immunity [26].



In this study, we have developed a promising strategy to rapidly manufacture InP-derived self-adjuvant, self-carrier, and self-assembled vaccines for cancer immunotherapy. InP has been approved and used clinically as an immunomodulatory drug to treat viral infections for more than 50 years [14-16, 18]. Compared to other newly developed immunostimulants, InP is an inexpensive and well-tolerated drug with an excellent safety record. The oral dose of InP is generally 1-6 g/day for human use [18-20, 22]. The median lethal dose (LD50) of oral, subcutaneous, and intravenous administration of InP in mice is 188 mg/mouse, 59 mg/mouse and 31 mg/mouse, respectively [27]. In this study, nanofibrous vaccines Fe-Ace-O2, at a total dose of 1.5 mg/mouse, which is about one-fortieth of its subcutaneous LD50 value, trigger an effective antitumor immune response and inhibit tumor growth at distant site *in vivo*. Compared with other delivery systems, newly developed cancer vaccines using an approved InP drug are expected to have low barriers to clinical translation. Subcutaneous administration was adopted to investigate the anti-tumor efficacy of the self-assembled vaccine in this paper. Oral administration of cancer vaccines has received increasing attention in recent years due to its convenience [28]. We will further study the possibility of self-assembled vaccines derived from InP for oral cancer vaccines in the future because InP drug is often administered orally in clinical practice.

The synthesis temperature has a great influence on the particle size, when  $\text{FeCl}_3 \cdot 6\text{H}_2\text{O}$  and InP solutions are used as raw materials to prepare coordination complexes. When the synthesis temperature was reduced from room temperature to an ice bath, the particle length of coordination complexes decreased from about 20  $\mu\text{m}$  to about 4  $\mu\text{m}$ . This is because an increase in temperature generally increases the kinetic energy of the reactant molecules, causing them to move more quickly, increasing the frequency of collisions, raising the reaction rate, and resulting a larger particle size. While the decrease in temperature will reduce the kinetic energy of the reactant molecules, slow down the molecular movement, reduce the rate of the coordination reaction, and thus reduce the particle size. Moreover, the resulting self-assembled cancer vaccines can be tailored from microscale rods to nanoscale fibers and spheres using triblock copolymers (F127,  $\text{EO}_{102}\text{PO}_{70}\text{EO}_{102}$ ) and polyvinylpyrrolidone K 15 (PVP). Herein, F127 and PVP act as structure-directing agents and capping agents to regulate the shape and reduce the size during the synthesis of self-assembled cancer vaccines. F127 consists of hydrophobic poly(propylene oxide) chains and hydrophilic poly(ethylene oxide) chains. PVP is composed of hydrophobic polyvinyl part and hydrophilic pyrrolidone part. In the synthetic aqueous solution of cancer vaccines, F127 and PVP can form different micelle shapes to adjust the morphology of particle, and adsorb onto the surface of particles to inhibit their growth via the steric effect.

When cocultured with primary DCs derived from mice *in vitro*, nanofibrous self-assembled cancer vaccines efficiently enhance the expression of chemokine receptor CCR7, costimulatory molecules CD86, and H-2K<sup>b</sup>-SIINFEKL antigen cross-presentation, compared with other groups, which implies their potential application in cancer immunotherapy. Chemokine receptor CCR7, expressed by mature DCs et al., is reported to govern the homing of DCs from the peripheral tissues to lymphoid organs [29], which is a one of the key steps to prime T cell immune activation. Costimulatory molecules CD86, mainly expressed on various APCs including DCs, provides costimulatory signals indispensable for T cell activation and survival [30]. H-2K<sup>b</sup>-SIINFEKL represent OVA antigen-specific cross-presentation, that is, peptide epitope of OVA (SIINFEKL) is presented by MHC class I molecules (H-2K<sup>b</sup>). MHC class I molecules are necessary for cross-presentation of exogenous antigens and the prime of CD8<sup>+</sup> T-cell immune response [31].

*In vivo* experiments have further confirmed that nanofibrous self-assembled cancer vaccines exhibit the strongest efficacy among all groups, not only in promoting targeted lymph node delivery, but also in enhancing cross-presentation of tumor antigens. The homing of DCs, which have captured antigens from the peripheral

injection sites to lymph nodes, and the subsequent presentation of antigens to T cells in lymph nodes, play a pivotal role in initiating antigen-specific CD8<sup>+</sup> T-cell immune responses.

The anti-tumor efficacy of the self-assembled cancer vaccine has been effectively verified using a tumor-bearing mouse model. Due to the adjuvant properties of immunomodulatory drug InP, mice treated with the mixture of OVA and InP in free format (free OVA + InP group) exhibit smaller tumor volume than mice treated with saline or free OVA. Due to the dual function of Fe-Ace coordination complexes simultaneously as adjuvants and carriers for tumor antigens, microscale self-assembled vaccines and nanofibrous self-assembled vaccines more effectively inhibit tumor growth than free OVA + InP group. Furthermore, due to the dual effects of nanosize effect and fibrous structure effect, nanofibrous self-assembled vaccines more effectively inhibit tumor growth than microscale self-assembled vaccines and nanospherical self-assembled vaccines.

Antitumor mechanism of self-assembled cancer vaccines has been comprehensively clarified using flow cytometry analysis of immune cell populations in key immune organs, immunohistochemical, immunofluorescent and conventional staining analysis, ELISA analysis and so on. Mice vaccinated with nanofibrous self-assembled vaccines exhibit higher percentages of CD4<sup>+</sup> and tetramer<sup>+</sup> in CD3<sup>+</sup>CD8<sup>+</sup> T cells in splenocytes, and higher percentages of CD4<sup>+</sup>, CD8<sup>+</sup> and tetramer<sup>+</sup>CD8<sup>+</sup> T cells in lymphocytes, compared with free OVA + InP group, microscale self-assembled vaccines and nanospherical self-assembled vaccines. Moreover, tumor sections of mice treated with nanofibrous self-assembled vaccines demonstrates less highly proliferative tumor cells, higher levels of apoptosis, larger necrosis regions and greater numbers of M1 macrophages, than other groups. CD4<sup>+</sup> T cells are generally thought to help CD8<sup>+</sup> T cells to mediate antitumor immunity, by directly activating CD8<sup>+</sup> T cells by secreting IL-2, or indirectly inducing CD8<sup>+</sup> T cell responses by supporting pro-inflammatory cross-presenting DCs [32]. Recently, CD4<sup>+</sup> T cells have also been reported to have direct antitumor activity through the production of cytokines such as IFN- $\gamma$  and TNF- $\alpha$  [32]. Cytotoxic CD8<sup>+</sup> T cells are the most critical part of the adaptive immunity and the most powerful effector cells in the antitumor immunity to directly destroy tumor cells by secreting cytokines and releasing perforin, granzymes and so on [33]. Here, tetramer<sup>+</sup> in CD3<sup>+</sup>CD8<sup>+</sup> T cells and tetramer<sup>+</sup>CD8<sup>+</sup> T cells all represent tumor antigen OVA - specific CD8<sup>+</sup> T cells. Nanofibrous self-assembled vaccines more effectively enhance the percentages of CD4<sup>+</sup>, CD8<sup>+</sup>, tetramer<sup>+</sup> in CD3<sup>+</sup>CD8<sup>+</sup> and tetramer<sup>+</sup>CD8<sup>+</sup> T cells in immune organs than other groups, which explains their superior antitumor efficacy over others. The facts that T cell depletion by anti-mouse CD8a antibody leads to rapid tumor growth further confirm that nanofibrous self-assembled cancer vaccines rely on CD8<sup>+</sup> T cells to exert anti-tumor immunity.

Overall, nanofibrous self-assembled vaccines most effectively promote the activation of DCs *in vitro*, enhance targeted lymph node delivery and antigen cross-presentation *in vivo*, trigger the cellular immune response to inhibit the distant tumor growth in tumor-bearing mouse models. The activation of APCs, including DCs and macrophages, and other immune cells have been reported to be highly dependent on the particle morphology of adjuvants and/or delivery system [9, 34-36]. For example, AlOOH adjuvants with long-rod shape more effectively induce DCs activation, such as high expression of CD86/CD80, and the production of cytokines, such as IL-1 $\beta$  and IL-6, than those with short-rod shape [34]. Hydroxyapatite particles with needle shape promote much higher IL-1 $\beta$  cytokine secretion by macrophage than those with spherical shape [37]. Compared with spherical structures, nanofibrous structures were reported to effectively drive the immune response toward Th1 type, which plays indispensable roles in antitumor immunity [38]. *In vivo* lymph nodes targeting of self-assembled cancer vaccine is also highly correlated with their particle size and shape [36]. Due to the size effect, nanoscale particles are easier to achieve lymph node targeting than microscale particles [36]. That's why



nanofibrous self-assembled vaccines and nanospherical self-assembled vaccines exhibit higher percentages of F-OVA<sup>+</sup> in CD11c<sup>+</sup> in lymph node than microscale self-assembled vaccines. In addition, due to fibrous structure effect, nanofibrous self-assembled vaccines induce DCs activation and the expression of chemokine receptor CCR7 more strongly than nanospherical self-assembled vaccines, which accounts for the stronger lymph node targeting ability of nanofibrous vaccines. In this study, both nanoscale and fibrous morphology of nanofibrous self-assembled vaccines should account for their stronger anti-tumor immune effects than other self-assembled vaccines, including microscale self-assembled vaccines and nanospherical self-assembled vaccines.

#### 4. Conclusion

In summary, we have developed a rapid method for the preparation of self-adjuvant, self-carrier and self-assembled cancer vaccines due to the coordination interaction of Fe<sup>3+</sup> and acedoben in InP. During the preparation process, model tumor antigen was uniformly encapsulated in Fe-Ace coordination complexes at the nanoscale. Meanwhile, the self-assembled cancer vaccines can be readily adjusted from the microscale to the nanoscale, with shapes including rods, fibers, and spheres. Herein, Fe-Ace coordination complexes not only serve as carriers for tumor antigens, but also strengthen antigen-specific antitumor immunity based on their intrinsic adjuvant properties. Fe-Ace coordination complexes facilitate the cellular uptake of tumor antigens by dendritic cells *in vitro*. Most importantly, the combination of acedoben with iron species significantly augmented its immune activation effect. Compared with InP in free format, self-assembled cancer vaccines based on Fe-Ace coordination complexes effectively triggered antitumor immune responses, exerted a remarkable therapeutic efficacy, and inhibited the tumor growth at distant site *in vivo*. The presented work presents a promising strategy for the rapid manufacture of InP-derived cancer vaccines for cancer immunotherapy.

#### Acknowledgements

We thank Dr. H. Yasufuku and Mr. S. Soeya for XPS measurement. We are also grateful to Dr. T. Takemura, Dr. X.L. Li, Dr. A. Yamamoto, Dr. Y. Shirai, and Ms. S. Kohara for their kind assistance during the experiments. We gratefully acknowledge the financial support from Japan Society for the Promotion of Science (JSPS, KAKENHI Grant No. 23K04555 and 22K20517), Takeda Science Foundation and NIMS funds. This work was supported in part by "Advanced Research Infrastructure for Materials and Nanotechnology in Japan (ARIM)" of the Ministry of Education, Culture, Sports, Science and Technology (MEXT), Japan. Proposal Number JPMXP1223NM5201.

#### References

- [1] A.S. Shavkunov, M.M. Gubin. The dynamics of an immunotherapy duo. *Nat Cancer*. 3 (2022) 376-378. <https://doi.org/10.1038/s43018-022-00362-5>.
- [2] X. Li, T. Yamazaki, M. Ebara, N. Shirahata, N. Hanagata. Nanoengineered coordination polymers boost cancer immunotherapy. *Mater Today*. 67 (2023) 127-150. <https://doi.org/10.1016/j.mattod.2023.06.001>.
- [3] M.H. Yu, W. Yang, W.W. Yue, Y. Chen. Targeted cancer immunotherapy: Nanoformulation engineering and clinical translation. *Adv Sci*. 9 (2022) 2204335. <https://doi.org/10.1002/advs.202204335>.
- [4] C.H. June, R.S. O'Connor, O.U. Kawalekar, S. Ghassemi, M.C. Milone. CAR T cell immunotherapy for human cancer. *Science*. 359 (2018) 1361-1365. <https://doi.org/10.1126/science.aar6711>.
- [5] A. Ribas, J.D. Wolchok. Cancer immunotherapy using checkpoint blockade. *Science*. 359 (2018) 1350-1355. <https://doi.org/10.1126/science.aar4060>.
- [6] U. Sahin, O. Tureci. Personalized vaccines for cancer immunotherapy. *Science*. 359 (2018) 1355-1360. <https://doi.org/10.1126/science.aar7112>.
- [7] P.A. Ott, Z.T. Hu, D.B. Keskin, S.A. Shukla, J. Sun, D.J. Bozym, W.D. Zhang, A. Luoma, A. Giobbie-Hurder,

- L. Peter, C. Chen, O. Olive, T.A. Carter, S.Q. Li, D.J. Lieb, T. Eisenhaure, E. Gjini, J. Stevens, W.J. Lane, I. Javeri, K. Nellaiappan, A.M. Salazar, H. Daley, M. Seaman, E.I. Buchbinder, C.H. Yoon, M. Harden, N. Lennon, S. Gabriel, S.J. Rodig, D.H. Barouch, J.C. Aster, G. Getz, K. Wucherpennig, D. Neuberg, J. Ritz, E.S. Lander, E.F. Fritsch, N. Hacohen, C.J. Wu. An immunogenic personal neoantigen vaccine for patients with melanoma. *Nature*. 547 (2017) 217-221. <https://doi.org/10.1038/nature22991>.
- [8] I. Melero, G. Gaudemack, W. Gerritsen, C. Huber, G. Parmiani, S. Scholl, N. Thatcher, J. Wagstaff, C. Zielinski, I. Faulkner, H. Mellstedt. Therapeutic vaccines for cancer: an overview of clinical trials. *Nat Rev Clin Oncol*. 11 (2014) 509-524. <https://doi.org/10.1038/nrclinonc.2014.111>.
- [9] X. Li, X. Wang, A. Ito. Tailoring inorganic nanoadjuvants towards next-generation vaccines. *Chem Soc Rev*. 47 (2018) 4954-4980. <https://doi.org/10.1039/c8cs00028j>.
- [10] M.S. Goldberg. Immunoengineering: How nanotechnology can enhance cancer immunotherapy. *Cell*. 161 (2015) 201-204. <https://doi.org/10.1016/j.cell.2015.03.037>.
- [11] H. Wang, D.J. Mooney. Biomaterial-assisted targeted modulation of immune cells in cancer treatment. *Nat Mater*. 17 (2018) 761-772. <https://doi.org/10.1038/s41563-018-0147-9>.
- [12] D. Irvine. Material aid for vaccines. *Nat Mat*. 17 (2018) 472-473. <https://doi.org/10.1038/s41563-018-0089-2>.
- [13] X. Li, S. Hattori, M. Ebara, N. Shirahata, N. Hanagata. A facile approach to preparing personalized cancer vaccines using iron-based metal organic framework. *Front Immunol*. 14 (2024) 1328379. <https://doi.org/10.3389/fimmu.2023.1328379>.
- [14] J. Sliva, C.N. Pantzartzi, M. Votava. Inosine pranobex: a key player in the game against a wide range of viral infections and non-infectious diseases. *Adv Ther*. 36 (2019) 1878-1905. <https://doi.org/10.1007/s12325-019-00995-6>.
- [15] M. Talpaz, W. Wong, J. Medina, H. Goepfert, G. Mavligit. The immune restorative effect of isoprinosine administration on the local graft-versus-host reaction of cancer patients. *Clin Immunol Immunop*. 28 (1983) 96-100. [https://doi.org/10.1016/0090-1229\(83\)90192-7](https://doi.org/10.1016/0090-1229(83)90192-7).
- [16] D.M. Campolirichards, E.M. Sorkin, R.C. Heel. Inosine pranobex - a preliminary review of Its pharmacodynamic and pharmacokinetic properties, and therapeutic efficacy. *Drugs*. 32 (1986) 383-424. <https://doi.org/10.2165/00003495-198632050-00001>.
- [17] D.J. Zahariy Krastev, Radina Ivanova. Isoprinosine induces a rapid lympho - mononuclear response in adult participants. *MedInform*. 2 (2015) 80-85. <https://doi.org/10.18044/MedInform.201521>.
- [18] C.R. Jayanthi, A.K. Swain, R.T. Ganga, D. Halnor, A. Avhad, M.S. Khan, A. Ghosh, S.S. Choudhary, A.N. Yannawar, S. Deshpande, M. Patel, K.P. Anne, Y. Bangar. Efficacy and safety of inosine pranobex in COVID-19 patients: a multicenter phase 3 randomized double-blind, placebo-controlled trial. *Adv Ther*. (2022) 2200159. <https://doi.org/10.1002/adtp.202200159>.
- [19] Q.D. Mu, L.Y. Chen, X.T. Gao, S.Y. Shen, W.J. Sheng, J.X. Min, F.D. Wang. The role of iron homeostasis in remodeling immune function and regulating inflammatory disease. *Sci Bull*. 66 (2021) 1806-1816. <https://doi.org/10.1016/j.scib.2021.02.010>.
- [20] S. Zanganeh, G. Hutter, R. Spitler, O. Lenkov, M. Mahmoudi, A. Shaw, J.S. Pajarinen, H. Nejadnik, S. Goodman, M. Moseley, L.M. Coussens, H.E. Daldrup-Link. Iron oxide nanoparticles inhibit tumour growth by inducing pro-inflammatory macrophage polarization in tumour tissues. *Nat Nanotechnol*. 11 (2016) 986-994. <https://doi.org/10.1038/nnano.2016.168>.
- [21] S.E. Kim, L. Zhang, K. Ma, M. Riegman, F. Chen, I. Ingold, M. Conrad, M.Z. Turker, M. Gao, X. Jiang, S. Monette, M. Pauliah, M. Gonen, P. Zanzonico, T. Quinn, U. Wiesner, M.S. Bradbury, M. Overholtzer. Ultrasmall nanoparticles induce ferroptosis in nutrient-deprived cancer cells and suppress tumour growth. *Nat Nanotechnol*. 11 (2016) 977-985. <https://doi.org/10.1038/nnano.2016.164>.
- [22] P. Santiago. Ferrous versus ferric oral iron formulations for the treatment of iron deficiency: a clinical overview. *Sci World J* 2012 (2012) 846824. <https://doi.org/10.1100/2012/846824>.
- [23] X. Li, X.P. Wang, A. Ito, N.M. Tsuji. A nanoscale metal organic frameworks-based vaccine synergises with PD-1 blockade to potentiate anti-tumour immunity. *Nat Commun*. 11 (2020) 3858. <https://doi.org/10.1038/s41467-020-17637-z>.
- [24] D. Liu, B. Deng, Z.R. Liu, B. Ma, X.G. Leng, D.L. Kong, T.J. Ji, L.X. Liu. Enhanced antitumor immune responses via a self-assembled carrier-free nanovaccine. *Nano Lett*. 21 (2021) 3965-3973. <https://doi.org/10.1021/acs.nanolett.1c00648>.
- [25] H.J. Song, Q. Su, W.F. Shi, P.S. Huang, C.N. Zhang, C. Zhang, Q. Liu, W.W. Wang. Antigen epitope-

- TLR7/8a conjugate as self-assembled carrier-free nanovaccine for personalized immunotherapy. *Acta Biomater.* 141 (2022) 398-407. <https://doi.org/10.1016/j.actbio.2022.01.004>.
- [26] X.Q. Sun, Y. Zhang, J.Q. Li, K.S. Park, K. Han, X.W. Zhou, Y. Xu, J. Nam, J. Xu, X.Y. Shi, L. Wei, Y.L. Lei, J.J. Moon. Amplifying STING activation by cyclic dinucleotide-manganese particles for local and systemic cancer metalloimmunotherapy. *Nat Nanotechnol.* 16 (2021) 1260-1270. <https://doi.org/10.1038/s41565-021-00962-9>.
- [27] <https://go.drugbank.com/drugs/DB13156>.
- [28] M. Gambirasi, A. Safa, I. Vruzhaj, A. Giacomini, F. Sartor, G. Toffoli. Oral administration of cancer vaccines: challenges and future perspectives. *Vaccines.* 12 (2024) 12010026. <https://doi.org/10.3390/vaccines12010026>.
- [29] R. Forster, A.C. Davalos-Misslitz, A. Rot. CCR7 and its ligands: balancing immunity and tolerance. *Nat Rev Immunol.* 8 (2008) 362-371. <https://doi.org/10.1038/nri2297>.
- [30] G. Baravalle, H. Park, M. McSweeney, M. Ohmura-Hoshino, Y. Matsuki, S. Ishido, J.S. Shin. Ubiquitination of CD86 is a key mechanism in regulating antigen presentation by dendritic cells. *J Immunol.* 187 (2011) 2966-2973. <https://doi.org/10.4049/jimmunol.1101643>.
- [31] O.P. Joffre, E. Segura, A. Savina, S. Amigorena. Cross-presentation by dendritic cells. *Nat Rev Immunol.* 12 (2012) 557-569. <https://doi.org/10.1038/nri3254>.
- [32] R.E. Tay, E.K. Richardson, H.C. Toh. Revisiting the role of CD4<sup>+</sup> T cells in cancer immunotherapy - new insights into old paradigms. *Cancer Gene Ther.* 28 (2021) 5-17. <https://doi.org/10.1038/s41417-020-0183-x>.
- [33] H. Raskov, A. Orhan, J.P. Christensen, I. Gogenur. Cytotoxic CD8<sup>+</sup> T cells in cancer and cancer immunotherapy. *Brit J Cancer.* 124 (2021) 359-367. <https://doi.org/10.1038/s41416-020-01048-4>.
- [34] B.B. Sun, Z.X. Ji, Y.P. Liao, M.Y. Wang, X. Wang, J.Y. Dong, C.H. Chang, R.B. Li, H.Y. Zhang, A.E. Nel, T. Xia. Engineering an effective immune adjuvant by designed control of shape and crystallinity of aluminum oxyhydroxide nanoparticles. *ACS Nano.* 7 (2013) 10834-10849. <https://doi.org/10.1021/nn404211j>.
- [35] X. Wang, X. Li, A. Ito, Y. Watanabe, N.M. Tsuji. Rod-shaped and fluorine-substituted hydroxyapatite free of molecular immunopotentiators stimulates anti-cancer immunity in vivo. *Chem Commun.* 52 (2016) 7078-7081. <https://doi.org/10.1039/c6cc02848a>.
- [36] X.P. Wang, S. Ihara, X. Li, A. Ito, Y. Sogo, Y. Watanabe, A. Yamazaki, N.M. Tsuji, T. Ohno. Rod-scale design strategies for immune-targeted delivery system toward cancer immunotherapy. *ACS Nano.* 13 (2019) 7705-7715. <https://doi.org/10.1021/acsnano.9b01271>.
- [37] F. Lebre, R. Sridharan, M.J. Sawkins, D.J. Kelly, F.J. O'Brien, E.C. Lavelle. The shape and size of hydroxyapatite particles dictate inflammatory responses following implantation. *Sci Rep.* 7 (2017) 2922. <https://doi.org/10.1038/s41598-017-03086-0>.
- [38] R. Mammadov, G. Cinar, N. Gunduz, M. Goktas, H. Kayhan, S. Tohumeken, A.E. Topal, I. Orujalipoor, T. Delibasi, A. Dana, S. Ide, A.B. Tekinay, M.O. Guler. Virus-like nanostructures for tuning immune response. *Sci Rep.* 5 (2015) 16728. <https://doi.org/10.1038/srep16728>.